tvst

https://doi.org/10.1167/tvst.8.2.1

Article

Cross-Sectional and Longitudinal Assessment of the Ellipsoid Zone in Childhood-Onset Stargardt Disease

Preena Tanna[1,2,*], Michalis Georgiou[1,2,*], Rupert W. Strauss[1–3], Naser Ali[1,2], Neruban Kumaran[1,2], Angelos Kalitzeos[1,2], Kaoru Fujinami[1,2,4,5], and Michel Michaelides[1,2]

[1] UCL Institute of Ophthalmology, University College London, London, UK
[2] Moorfields Eye Hospital, London, UK
[3] Departments of Ophthalmology, Johannes Kepler University and Medical University Graz, Austria
[4] Division of Vision Research, National Institute of Sensory Organs, National Hospital Organization, Tokyo Medical Center, Tokyo, Japan
[5] Department of Ophthalmology, Keio University School of Medicine, Tokyo, Japan

Correspondence: Michel Michaelides, UCL Institute of Ophthalmology, 11-43 Bath St, London, EC1V 9EL, UK. e-mail: michel.michaelides@ucl.ac.uk

Received: 18 October 2018
Accepted: 12 December 2018
Published: 1 March 2019

Keywords: OCT; ellipsoid zone; EZ; retina; Stargardt disease; *ABCA4*; STGD1; clinical trials; endpoints

Citation: Tanna P, Georgiou M, Strauss RW, Ali N, Kumaran N, Kalitzeos A, Fujinami K, Michaelides M. Cross-sectional and longitudinal assessment of the ellipsoid zone in childhood-onset Stargardt disease. Trans Vis Sci Tech. 2019;8(2):1, https://doi.org/10.1167/tvst.8.2.1

Purpose: To evaluate the reliability of ellipsoid zone (EZ) loss width and area measurements from spectral-domain optical coherence tomography (SD-OCT) images and track disease progression in childhood-onset Stargardt disease (STGD1).

Methods: Children with molecularly confirmed STGD1 ($n = 46$, mean age 12.4 years) underwent SD-OCT for the measurement of the transverse (width) loss of the EZ and en face analysis to quantify the area of EZ loss. All scans were analyzed twice by two graders to evaluate reliability. The annual rate of EZ width and area loss were calculated.

Results: The intra- and intergrader reliability of transverse EZ loss and area of EZ loss measurements at baseline for both graders was 0.99. The mean annual rate of transverse EZ loss (±standard deviation) was 279.5 ± 259.9 μm/y. The mean rate of area of EZ loss (±standard deviation) was 1.20 ± 1.29 mm^2/y. The percentage transverse EZ loss was 10.2 ± 9.9%/y, which was significantly lower than the area of EZ loss at 19.4 ± 16.3%/y. High degree of interocular symmetry was observed.

Conclusions: This is a prospective study on the quantification of EZ loss in children with STGD1 and highlights the reliability of SD-OCT in measuring EZ loss. High intra- and intergrader reliability was observed, with good ability to detect changes over time.

Translational Relevance: Measuring the area of EZ loss was more sensitive compared with transverse EZ width loss measurements and will be valuable for natural history studies and clinical trials requiring sensitive and reliable structural endpoints.

Introduction

Stargardt disease (STGD1; Online Mendelian Inheritance in Man, 248200) is the most common inherited macular dystrophy with a prevalence of 1 in 8000 to 10,000.[1–7] Onset is most commonly in childhood where patients present with bilateral central visual loss and characteristic macular atrophy with yellow–white flecks at the level of the retinal pigment epithelium (RPE) at the posterior pole.[1,2,5,8,9] STGD1 has an autosomal-recessive mode of inheritance associated with disease-causing sequence variants in the ATP-binding cassette, subfamily A, member 4 (*ABCA4*) gene (Mendelian Inheritance in Man, 601691).[1,10–13] *ABCA4* encodes the retinal specific transmembrane protein,[14,15] which is localized to the rim of rod and cone outer segment discs and involved in the active transport of retinoids from photoreceptors to RPE.[14–16] ABCA4 dysfunction results in lipofuscin accumulation in the RPE[14,17,18] and toxic levels of lipofuscin in the RPE are associated with photoreceptor degeneration and ultimately RPE loss.[19–21]

A robust measurement of photoreceptor integrity is therefore crucial for monitoring disease progression and for the design of any treatment strategy. The

ellipsoid zone (EZ) is a hyperreflective layer in the outer retina and has been associated with photoreceptor integrity and function. Spectral-domain optical coherence tomography (SD-OCT) enables in vivo high-resolution cross-sectional retinal images, allowing for quantitative assessments of the EZ, including manual identification of the transverse EZ loss and delineation of the area of EZ loss from an en face image. The EZ has been characterized in STGD1,[22–24] yet only one study has tracked progression by the presence or absence of the EZ using en face OCT.[25]

Despite increasing evidence that early-onset STGD1 belongs to the severe end of the spectrum of *ABCA4*-associated retinal phenotypes,[4,7,26] no studies have assessed the EZ cross-sectionally or longitudinally in an exclusively pediatric population. Measuring photoreceptor layer integrity in children would be valuable in understanding the natural history of STGD1 in young patients and help determine whether children have better retinal potential for therapeutic intervention. Here, we evaluate the reliability of both the width of transverse loss of EZ and the area of EZ loss from en face SD-OCT analysis, as well as track disease progression to determine whether the EZ could serve as a robust anatomic outcome measure in children with molecularly confirmed STGD1.

Methods

This prospective observational study adhered to the tenets of the Declaration of Helsinki and was approved by the Moorfields Eye Hospital Ethics Committee. Informed consent and assent were obtained from parents and children, respectively, prior to entering the study.

Subjects

A total of 46 children (mean age at baseline, 12.4 years; range, 6–18) with molecularly confirmed STGD1, from 39 pedigrees, including 19 males and 27 females, were included in this study. Tables 1 and 2 summarizes the demographics and genetic findings for each subject.

SD-OCT Image Acquisition

All subjects underwent SD-OCT imaging using the Heidelberg Spectralis (Heidelberg Engineering, Heidelberg, Germany). A transfoveal horizontal line scan was acquired for the measurement of the extent of the transverse loss of the EZ. The protocol also included two horizontal volume scans centered at the fovea covering a $20° \times 20°$ area to enable an en face analysis for the measurement of the area of EZ loss. The first volume scan comprised 49 horizontal B-scans with 124-μm interscan spacing, and the second comprised of 193 horizontal B-scans with 31-μm interscan spacing. The SD-OCT scans were automatically registered to a near-infrared reflectance (NIR-R) fundus image, which was acquired simultaneously. All scans were obtained using the automatic retinal tracking (ART) mode and automatic registration was used for all follow-up scans.

SD-OCT Image Analysis

Images for each subject were analyzed using the Heidelberg Eye Explorer software (version 1.9.10.0; Heidelberg Engineering) and were displayed in the 1:1-μm setting. The acquired transfoveal horizontal line scan was used to measure the extent of the transverse loss of the EZ. The nasal and temporal location of the EZ loss, identified as the point where the hyperreflective EZ was no longer discernible/continuous, was manually demarcated with the arrow tool. The caliper tool was then used to delineate the width of the transverse loss of the EZ, which was automatically calculated by the software. In all patients, with the exception of P2, no residual EZ structure was visible between the nasal and temporal borders. For consistency we decided to measure the EZW in the same way in P2 with 'foveal sparing', as undertaken in the rest of the cohort.

The acquired macula volume scans and associated NIR-R fundus image were used for en face analysis to measure the extent of the area of EZ loss. En face analysis was done manually by assessing each individual B-scan. All B-scans had a quality index greater than 25 dB. The nasal and temporal location of the EZ loss for each consecutive B-scan was marked and the corresponding locations were annotated on the NIR-R fundus image. Once all the nasal and temporal borders were marked, the region finder tool was used to join the points delineating the area of EZ loss on the NIR-R fundus image and the area value was automatically calculated by the software. The denser scan, when available, was preferentially used for analysis. In a few patients the less dense scans were used because of better image quality (more reliable identification of EZ borders), because for the less dense scans it was easier to keep the ART at a higher value. In addition, having multiple scans at both baseline and follow-up made it easier to identify the exact same location for measuring EZW and track

Table 1. Genetics

Subject Number	Subject ID	Variant 1	
P1	MM_0020	c.4918C>T;c.4222T>C	p.Arg1640Trp;p.Trp1408Arg
P2	MM_0021	c.5882G>A	p.Gly1961Glu
P3	MM_0058	c.5882G>A	p.Gly1961Glu
P4	MM_0070	c.5882G>A;c.3758C>T	p.Gly1961Glu;p.Thr1253Met
P5	MM_0090	c.3322C>T	p.Arg1108Cys
P6	MM_0107	c.5161_5162delAC	p.Thr1721HisfsTer65
P7	MM_0130	c.768G>T	p.Val256Val, Splice site alteration
P8	MM_0138	*c.5898+2T>C*	*Splice site alteration*
P9	MM_0146	c.5196+1137G>A	Deep intronic change
P10	MM_0148	c.5461-10T>C	Splice site alteration
P11	MM_0230	c.4139C>T	p.Pro1380Leu
P12	MM_0227	*c.6391G>A*	*p.Glu2131Lys*
P13	MM_0258	c.4793C>A	p.Ala1598Asp
P14	MM_0286	c.4685T>C	p.Ile1562Thr
P15	MM_0281	c.4469G>A	p.Cys1490Tyr
P16	MM_0282	c.5461-10T>C	Splice-site alteration
P17	MM_0284	c.1253T>C	p.Phe418Ser
P18	MM_0312	c.3322C>T	p.Arg1108Cys
P19	MM_0326	c.214G>A	p.Gly72Arg
P20	MM_0356	c.1253T>C	p.Phe418Ser
P21	MM_0291	c.1648G>A	p.Gly550Arg
P22	MM_0026	c.5549T>C	p.Leu1850Pro
P23	MM_0225	c.4469G>A	p.Cys1490Tyr
P24	MM_0131	c.768G>T	p.Val256Val, splice-site alteration
P25	MM_0360	c.214G>A	p.Gly72Arg
P26	MM_0382	c.6445C>T	p.Arg2149Ter
P27	MM_0399	c.1622T>C; c.3113C>T	p.Leu541Pro;p.Ala1038Val
P28	MM_0421	*c.4571A>G*	*p.Asp1524Gly*
P29	MM_0431	c.6320G>A	p.Arg2107His
P30	MM_0432	c.4462T>C	p.Cys1488Arg
P31	MM_0240	*c.29_30insT*	*p.Leu10PhefsTer44*
P32	MM_0113	c.6817-2A>C	Splice-site alteration
P33	MM_0185	c.4918C>T;c.4222T>C	p.Arg1640Trp;p.Trp1408Arg
P34	MM_0246	c.5461-10T>C	Splice-site alteration
P35	MM_0260	*c.4539+2065C>G*	*Deep intronic change*
P36	MM_0314	c.5461-10T>C	Splice-site alteration
P37	MM_0108	c.5161_5162delAC	p.Thr1721HisfsTer65
P38	MM_0228	c.3113C>T;c.1622T>C	p.Ala1038Val;p.Leu541Pro
P39	MM_0241	c.3064G>A	p.Glu1022Lys
P40	MM_0426	c.6729+5_19delGTTGGCCCTGGGGCA	Splice-site alteration
P41	MM_0433	c.6729+5_19delGTTGGCCCTGGGGCA	Splice-site alteration
P42	MM_0351	c.1253T>C	p.Phe418Ser
P43	MM_0310	c.885delC	p.Asp295AspfsTer5
P44	MM_0267	c.4469G>A	p.Cys1490Tyr
P45	MM_0325	c.214G>A	p.Gly72Arg
P46	MM_0335	c.6319C>T	p.Arg2107Cys

Reference: NM_000350.2.
Novel variants are shown in italics.
Pathogenicity of novel variants was assessed with the previously reported methods.[11]

Table 1. Extended

Subject Number	Variant 2		Variant 3	
P1	*c.247_258insCAAA*	*p.Gln83ProfsTer17*		
P2	c.4793C>A	p.Ala1598Asp		
P3	c.454C>T	p.Arg152Ter		
P4	c.3364G>A	p.Glu1122Lys		
P5	c.3210_3211insGT	p.Ser1071CysfsTer14		
P6	c.2588G>C	p.Gly863Ala		
P7	c.634C>T	p.Arg212Cys		
P8	*c.286A>T*	*p.Asn96Tyr*		
P9	c.3364G>A	p.Glu1122Lys		
P10	c.3259G>A	p.Glu1087Lys		
P11	c.2588G>C	p.Gly863Ala		
P12	c.1957C>T	p.Arg653Cys	c.1411G>A	p.Glu471Lys
P13	c.2300T>A	p.Val767Asp		
P14	c.4469G>A	p.Cys1490Tyr	c.2588G>C	p.Gly863Ala
P15	c.3191-1G>T	Splice site alteration		
P16	c.4363T>C	p.Cys1455Arg		
P17	c.1253T>C	p.Phe418Ser		
P18	c.454C>T	p.Arg152Ter		
P19	c.214G>A	p.Gly72Arg		
P20	c.3322C>T	p.Arg1108Cys		
P21	c.4918C>T	p.Arg1640Trp		
P22	c.4469G>A	p.Cys1490Tyr		
P23	c.6449G>A	p.Cys2150Tyr		
P24	c.634C>T	p.Arg212Cys		
P25	c.214G>A	p.Gly72Arg		
P26	c.5018+5G>A	Splice-site alteration		
P27	c.5714+5G>A	Splice-site alteration		
P28	*c.4571A>G*	*p.Asp1524Gly*		
P29	*c.2385C>G*	*p.Ser795Arg*		
P30	c.5882G>A	p.Gly1961Glu		
P31				
P32	c.1906C>T	p.Gln636Ter		
P33	*c.247_250insCAAA*	*p.Gln83ProfsTer17*		
P34	*c.4326C>A*	*p.Asn1442Lys*		
P35	c.6118C>T	p.Arg2040Ter		
P36	c.4139C>T	p.Pro1380Leu		
P37	c.2588G>C	p.Gly863Ala		
P38				
P39	c.3064G>A	p.Glu1022Lys		
P40	c.6729+5_19delGTTGGCCCTGGGGCA	Splice-site alteration		
P41	c.6729+5_19delGTTGGCCCTGGGGCA	Splice-site alteration		
P42	c.4773+1G>T	Splice-site alteration		
P43	c.1804C>T	p.Arg602Trp		
P44	c.5318C>A	p.Ala1973Glu		
P45	c.214G>A	p.Gly72Arg		
P46	c.5461-10T>C	Splice site alteration		

rate of progression over time, especially in cases where the single line scans were not over the same exact location at follow-up visit.

Baseline and follow-up line and volume scans from both eyes were analyzed twice in a masked fashion by two graders (PT and MG) to determine the reliability of both EZ measurements. Graders were masked to their previous measurements, as well as the measurement of the other grader. Measurements were repeated at least 1 week apart. Both graders have practiced the method in 10 scans (data not used for the study). The results were comparable between graders and so it was decided to apply the method to the study. In terms of expertise, both graders are postgraduate students with 3 (PT) and 1.5 (MG) years of experience in clinical research in inherited retinal diseases (IRDs) and retinal imaging.

All measurements, both at baseline and follow-up, given their transverse nature, were corrected using the ratio between the assumed axial length of the OCT system (24 mm) and the actual axial length measurement for that eye (Zeiss IOL Master; Carl Zeiss Meditec, Dublin, CA).

Statistical Methods

The statistical analysis was carried out for transverse EZ loss measurements and area of EZ loss measurements using SPSS Statistics (Chicago). Significance for all statistical tests was set at $P < 0.05$. The Shapiro-Wilk test was used to test for normality for all variables.

A multilevel mixed-effects model was fitted with random grader and subject effects and intra- and intergrader reliability were assessed by the intraclass correlation coefficient (ICC). The annual rate of transverse EZ loss and area of EZ loss was calculated for each eye.

The interocular symmetry was assessed with paired *t*-test for both, area and width measurements, at baseline and follow-up as well as annual rates of EZ loss. Interocular correlation between eyes in the baseline measurements, follow-up measurements, and annual rate of transverse EZ loss and annual rate of area of EZ loss were assessed with Pearson's correlation coefficient.

The difference between eyes in the baseline measurement, follow-up measurement, and the annual rate of progression was assessed using the paired-samples *t*-test. The correlations between eyes were assessed with the Pearson's correlation coefficient. Subsequently, the strength of the correlations between the baseline measurement and annual rate of progression, baseline measurement, and age at baseline as well as the age at baseline and annual rate of progression were assessed with the Pearson's correlation coefficient. Strong, moderate, and weak correlation was set as $r > 0.7$, $0.7 > r > 0.5$, and $r < 0.5$, respectively.

Results

Thirty-eight subjects (P1–P38) underwent baseline testing on both eyes and contributed to the reliability analysis at baseline. The data from seven subjects (P39–P45) could not be analyzed as the baseline images showed the loss to extend beyond the SD-OCT scan limits. In contrast, subject P46 who was asymptomatic when recruited and was followed-up for 15 months, showed a healthy EZ at baseline and follow-up bilaterally, and thereby excluded from the analysis. Twenty-two of these subjects (P1–P22) also underwent follow-up testing on both eyes and contributed to the reliability analysis at follow-up to assess reliability at a later cross-section in time. Nine subjects either did not have follow-up visits ($n = 7$) or their EZ loss extended beyond the area imaged with OCT ($n = 2$), and thereby were excluded from longitudinal analysis. In patients P32 to P38 (Table 2), missing measurements are due to the EZ loss extending beyond the scan borders; with the exception of P37, which was due to poor compliance at baseline image acquisition. Some patients have only an EZW, because technically it was easier to center the lesion for a single line scan, and they thereby lack an EZ area because the whole area of the lesion was not imaged in the volume scans (e.g., P33 and P34). All measured variables were normally distributed. Table 2 summarizes all measurements.

Intragrader and Intergrader Reliability

Data from the right eye of all subjects were used for this analysis, after proving disease symmetry and in order to avoid any clustering effect. At baseline, the mean absolute difference in the transverse EZ loss on repeat measurement for grader 1 (PT) and grader 2 (MG) was 223.2 ± 178.5 and 176.4 ± 196.6 μm, respectively, and between graders after averaging their two sets of measurements was 161.3 ± 137.6 μm. The intragrader ICC at baseline for both graders and the intergrader ICC was 0.99. At follow-up, the mean absolute difference in the transverse EZ loss on repeat measurement for graders 1 and 2 was 279.5 ± 362.1 and 255.3 ± 331.6 μm, respectively, and

Table 2. Subject Demographics and Ellipsoid Zone Measurements

Subject Number	Age at Baseline, y	Sex	Follow-Up Time, mo	Width of Ellipsoid Zone Loss, μm				Area of Ellipsoid Zone Loss, mm^2			
				Baseline		Follow-up		Baseline		Follow-Up	
				Right Eye	Left Eye	Right Eye	Left Eye	Right Eye	Left Eye	Right Eye	Left Eye
P1	8	F	52	3615	3524	4152	4090	6.7	7.24	10.92	11.34
P2[a]	15	M	51	2118	2466	3209	2976	3.66	3.55	4.67	4.52
P3	16	M	22	1630	1678	1623	1720	0.95	1.2	1.26	1.29
P4	16	F	23	1637	1472	1931	1789	1.81	1.41	2.11	2.14
P5	14	F	38	3289	2749	3694	3674	5.68	5.86	7.99	7.33
P6	16	F	44	1235	1175	1395	1360	0.71	0.85	0.97	0.96
P7	8	M	24	984	1071	1263	1222	0.45	0.49	1.14	0.95
P8	8	M	29	3359	2553	3834	3598	6.21	6.19	8.18	7.7
P9	17	F	30	2901	2517	3546	3775	3.87	4.06	8.7	9.41
P10	15	F	27	3462	3838	4172	3860	7.97	8.55	9.07	9.46
P11	16	F	23	966	998	1019	1063	0.51	0.54	0.51	0.58
P12	14	F	25	991	1472	1420	19811	0.47	1.27	1.78	2.02
P13	15	F	12	3619	2678	3919	3302	8.24	7.76	9.38	8.52
P14	17	M	12	3413	3576	3698	3772	5.33	5.49	6.07	6.47
P15	9	F	12	3975	3953	4504	4277	9.59	9.17	12.1	12.31
P16	11	F	25	4337	3416	4664	4740	10.61	9.49	12.85	12.07
P17	12	M	24	3803	3813	3681	3827	8.04	7.74	8.33	8.28
P18	11	F	18	3611	3448	4897	4752	9.29	9.55	10.9	12.61
P19	8	M	17	4075	3830	4159	4201	9.01	8.06	10.78	9.98
P20	10	M	12	1323	1215	1469	1465	0.76	0.76	1	0.96
P21	13	M	13	1693	1972	3550	2980	3.17	3.86	4.04	4.9
P22	11	F	40	3623	3725	4022	3969	9.61	8.78	12.11	10.67
P23	8	M	NA	5009	4809	NA[b]	NA[b]	17.41	18.12	NA[b]	NA[b]
P24	10	F	NA	714	787	NA[c]	NA[c]	0.24	0.21	NA[c]	NA[c]
P25	8	F	NA	3811	4451	NA[c]	NA[c]	13.11	13.29	NA[c]	NA[c]
P26	11	F	NA	2829	3200	NA[c]	NA[c]	4.35	4.93	NA[c]	NA[c]
P27	17	F	NA	5311	5767	NA[c]	NA[c]	15.06	15.89	NA[c]	NA[c]
P28	14	F	NA	5590	5408	NA[b]	NA[b]	14.98	16.19	NA[b]	NA[b]
P29	17	M	NA	3909	3729	NA[c]	NA[c]	9.5	10.21	NA[c]	NA[c]
P30	17	M	NA	648	776	NA[c]	NA[c]	0.29	0.28	NA[c]	NA[c]
P31	10	M	NA	2540	2520	NA[c]	NA[c]	4.27	4.26	NA[c]	NA[c]
P32	17	F	35	3336	3473	4721	5471	6.77	6.96	18.99	22.45
P33	6	F	32	4235	4536	4996	5277	9.86	10.14	17.89	NA[b]
P34	12	M	27	5389	4786	5509	6034	18.57	15.18	23.31	NA[b]
P35	12	F	27	4973	4646	NA[b]	5165	13.91	12.66	NA[b]	14.95
P36	15	F	17	4478	5074	5428	NA[b]	10.51	12.43	17.61	NA[b]
P37	12	F	44	NA[b]	964	1183	1184	NA[b]	0.58	0.58	0.69
P38	14	F	29	4972	NA[b]	5573	5336	15.62	NA[b]	20.8	19.07
P39	18	F	NA	NA[b]	NA[b]	NA[b]	NA[b]	NA[b]	NA[b]	NA[b]	NA[b]
P40	8	M	NA	NA[b]	NA[b]	NA[b]	NA[b]	NA[b]	NA[b]	NA[b]	NA[b]
P41	12	M	NA	NA[b]	NA[b]	NA[b]	NA[b]	NA[b]	NA[b]	NA[b]	NA[b]
P42	10	M	NA	NA[b]	NA[b]	NA[b]	NA[b]	NA[b]	NA[b]	NA[b]	NA[b]
P43	8	M	NA	NA[b]	NA[b]	NA[b]	NA[b]	NA[b]	NA[b]	NA[b]	NA[b]

Table 2. Continued

Subject Number	Age at Baseline, y	Sex	Follow-Up Time, mo	Width of Ellipsoid Zone Loss, μm				Area of Ellipsoid Zone Loss, mm^2			
				Baseline		Follow-up		Baseline		Follow-Up	
				Right Eye	Left Eye	Right Eye	Left Eye	Right Eye	Left Eye	Right Eye	Left Eye
P44	12	M	NA	NA[b]	NA[b]	NA[b]	NA[b]	NA[b]	NA[b]	NA[b]	NA[b]
P45	9	F	NA	NA[b]	NA[b]	NA[b]	NA[b]	NA[b]	NA[b]	NA[b]	NA[b]
P46	14	F	15	NA[b]	NA[b]	NA[b]	NA[b]	NA[b]	NA[b]	NA[b]	NA[b]

F, female; M, male; NA, not available.
[a] Foveal Sparing.
[b] Ellipsoid Zone loss extending beyond the border of the scans.
[c] No follow-up visits available.

between graders, after averaging their two sets of measurements, was 89.6 ± 79.1 μm. The intragrader ICC at follow-up for both graders was 0.98, and intergrader ICC was 0.99.

At baseline, the mean absolute difference in the area of EZ loss on repeat measurement for graders 1 and 2 was 0.42 ± 0.38 and 0.41 ± 0.39 mm^2, respectively, and between graders, after averaging their two sets of measurements, was 0.28 ± 0.33 mm^2. The intragrader ICC at baseline for both graders and the intergrader ICC was 0.99. At follow-up, the mean absolute difference in the area of EZ loss on repeat measurement for graders 1 and 2 was 0.43 ± 0.38 and 0.55 ± 0.76 mm^2, respectively, and between graders, after averaging their two sets of measurements, was 0.23 ± 0.24 mm^2. The intragrader and the intergrader ICC at follow-up for both graders was 0.99.

Interocular Symmetry

Data from the 22 subjects (P1–P22) with baseline and follow-up testing on both eyes were analyzed further to assess interocular symmetry.

The mean absolute difference after averaging all four baseline measurements (2 from each observer) of the transverse EZ loss between eyes was 289.0 ± 291.3 μm; and in the follow-up measurement was 176.4 ± 168.5 μm. The mean difference in the annual rate of transverse EZ loss between eyes was 158.9 ± 194.6 μm/y. There was no statistically significant difference between eyes in the baseline measurement ($P = 0.092$), follow-up measurement ($P = 0.209$), and annual rate of EZ loss width ($P = 0.726$). There was a strong positive correlation between eyes in the baseline measurement ($r = 0.95$), follow-up measurement ($r = 0.98$), and annual rate of transverse EZ loss ($r = 0.75$).

The mean absolute difference in the baseline measurements of the area of EZ loss between eyes was 0.39 ± 0.33 mm^2 and in the follow-up measurement was 0.48 ± 0.46 mm^2. The mean difference in the annual rate of area of EZ loss between eyes was 0.21 ± 0.22 mm^2/y. There was no statistically significant difference between eyes in the baseline measurement ($P = 0.75$), follow-up measurement ($P = 0.923$), and annual rate of area of EZ loss ($P = 0.424$). There was a strong positive correlation between eyes in the baseline measurement ($r = 0.99$), follow-up measurement ($r = 0.99$), and annual rate of area of EZ loss ($r = 0.94$) (Fig. 1).

Rate of Progression

A total of 29 subjects (P1–P22, P32–P38; mean age at baseline, 12.7 years; range, 6–17) with both baseline and follow-up testing on at least one eye were included to determine the annual rate of progression. In subjects with testing on both eyes, one eye was chosen at random, given the symmetry between eyes, for the examined parameters. The mean follow-up period for this subgroup was 27 months (range, 12–52 months). Figure 2 shows representative examples of the variability in progression.

The mean annual rate of transverse EZ loss was 279.5 ± 259.9 μm/y. The mean baseline measurement of the transverse EZ loss was 2939.9 ± 1294.0 μm. There was a weak positive correlation ($r = 0.15$) between the baseline measurement and the annual rate of transverse EZ loss, and a weak negative correlation ($r = -0.21$) between the baseline measurement and age at baseline. There was no correlation

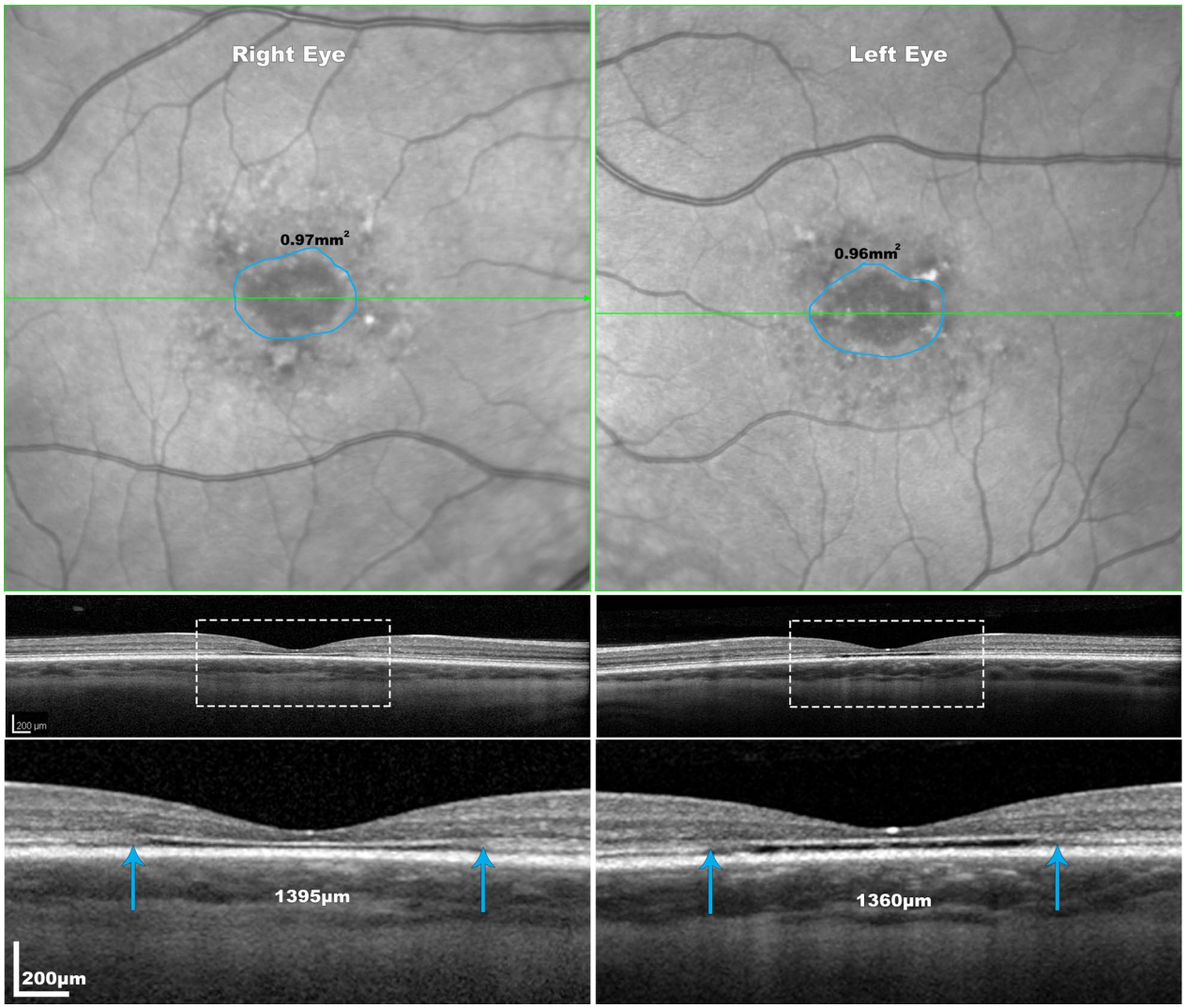

Figure 1. Representation of interocular symmetry of EZ loss measurements of a 20 years old female (P6) with STGD1 at the 4 years follow-up visit. The areas of EZ loss are delineated with blue lines on the NIR-R images and the area imaged in the OCT B-scan below is represented with *blue arrows*. The *blue arrows* on the OCT images mark the boundaries of the EZ loss. The disease shows high interocular symmetry in this individual. All images on the first two rows are at the same scale. The delineated areas with the *white rectangle* are magnified (×3) in the third row.

between the age at baseline and annual rate of transverse EZ loss ($r = -0.01$).

The mean annual rate of area of EZ loss was 1.20 ± 1.29 mm^2/y. The mean baseline measurement of area of EZ loss was 6.43 ± 4.67 mm^2. There was a strong moderate positive correlation ($r = 0.55$) between the baseline measurement and the annual rate of area of EZ loss, and a weak negative correlation ($r = -0.22$) between the baseline measurement and age at baseline. There was no correlation between the age at baseline and annual rate of area of EZ loss ($r = -0.03$) (Fig. 2).

The mean annual rates of transverse EZ loss and area of EZ loss were 10.2 ± 9.9%/y and 19.4 ± 16.3 %/y respectively, which were significantly different ($P = 0.004$). Figure 3 illustrates the variability in the percentage annual rate of loss.

Discussion

This is the first prospective study on the characterization of the EZ in a large cohort of molecularly confirmed children with STGD1. The high intra- and intergrader ICCs of both the transverse EZ loss and area of EZ loss measurements, as well as the ability to

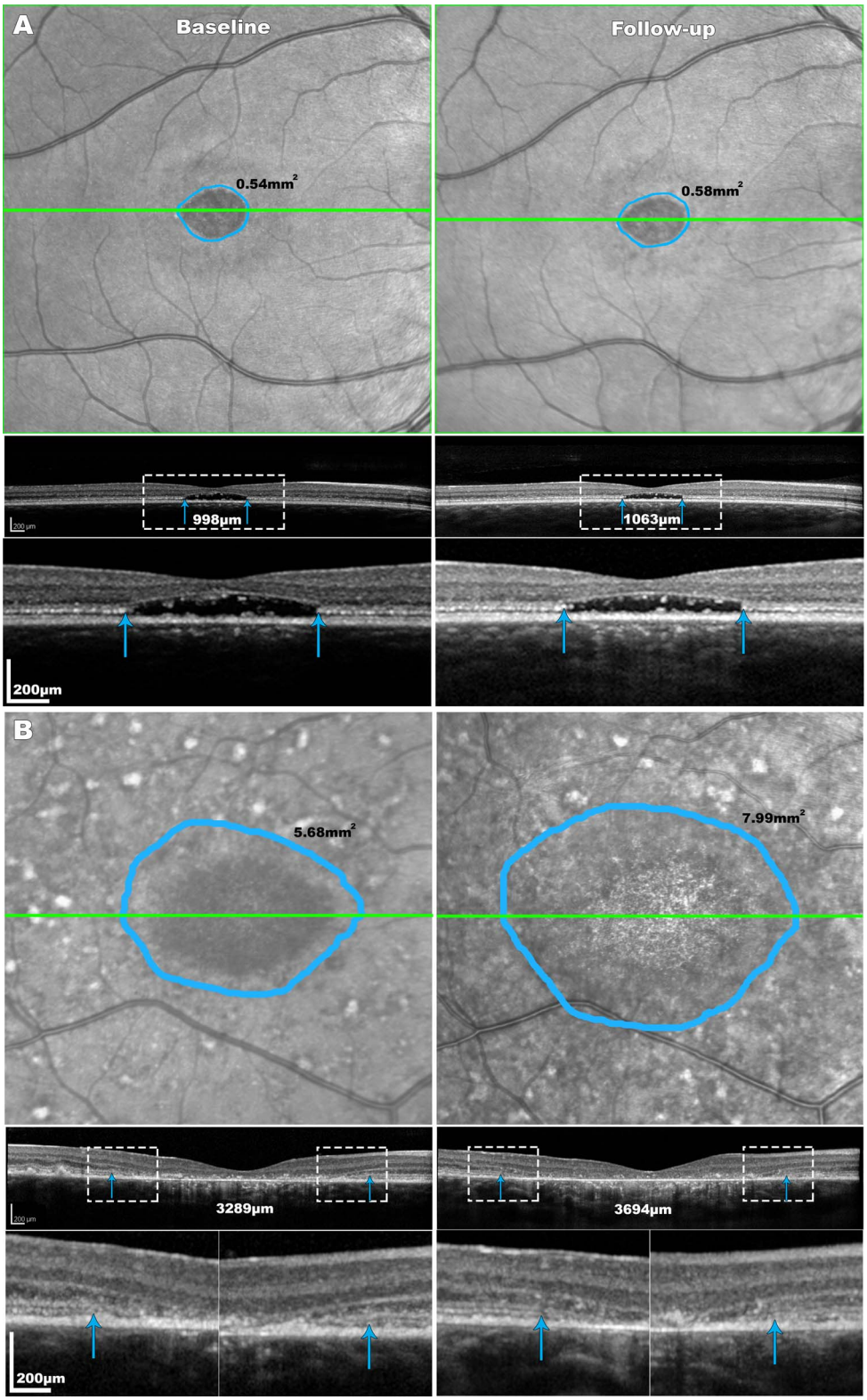

Figure 2. Disease progression in two STGD1 patients. The areas of EZ loss are delineated with *blue lines* on the NIR-R images and the section imaged in the OCT B-scan below is represented with *green lines*. The *blue arrows* on the OCT images mark the boundaries of the EZ loss. Patient (A) is a 16-years-old female (P11) with 24 months of follow-up. The disease was relatively stable for that patient with an annual rate of EZ area loss of 0.02 mm^2 and of EZ width expansion of 33 µm/y. Patient (B) is a 14-year-old female (P5) with rapid disease progression over 38 months, with an annual rate of EZ area loss of 0.73 mm^2 and of EZ width loss of 128 µm. The delineated areas with the *white rectangles* are magnified (×3) in the third row of panels (A) and (B).

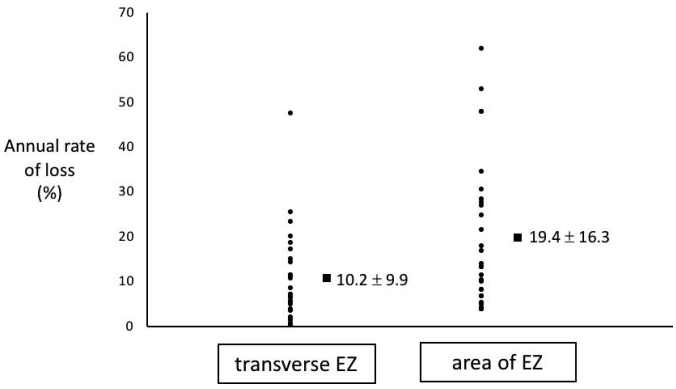

Figure 3. Stacked scatterplot showing the variability of the percentage annual rate of change in transverse EZ loss and area of EZ loss. Values represent mean ± SD.

detect change over time, suggests the EZ could serve as a robust anatomic outcome measure in children.

There are no studies in children with STGD1 on the quantification of EZ loss both cross-sectionally, and longitudinally to determine rates of progression. One study that characterized the baseline transverse EZ loss in STGD1 subjects (mean age 34.4 years) showed the mean measurement was 3911 ± 1423 μm.[27] In our study, although the mean age of the cohort was notably younger (mean age 12.4 years), the mean baseline measurement of the transverse EZ loss was comparable (2939.9 ± 1294.0 μm). However, no studies have previously assessed rate of progression of the transverse EZ loss over time in STGD1.

Only one study has assessed the area of EZ loss longitudinally in STGD1 subjects (mean age 33.0 years) and demonstrated a gradual expansion in the area of EZ loss of 0.31 mm^2/y, with the mean (± standard deviation) initial area of EZ loss being 4.18 ± 1.91 mm^2.[25] In contrast, our study identified a higher mean baseline measurement (6.43 ± 4.67 mm^2), and notably the mean annual rate of area of EZ loss was more than 3 times faster (1.20 ± 1.29 mm^2/year). This is likely to be due to our cohort having earlier-onset disease associated with more rapid progression than adult cohorts.[4] This is also supported by the relatively high proportion (52%) of subjects harboring severe disease-causing variants in our cohort that would be expected to affect splicing, or to introduce a premature truncating codon in the protein if translated.

All measurements were higher than the inherent variability in measurements taken from Spectralis images (lateral optical resolution = 14 μm). However, the data from seven subjects (P39–P45) were excluded as the baseline images showed the loss to extend beyond the limits of the SD-OCT scan. Six of these subjects were aged 12 or younger at baseline. This indicates that the phenotype can be variable, with highly progressive disease from early childhood, highlighting the importance of analyzing children and adults independently, and there is a group of children who have very rapidly progressive disease who would be ideal for clinical trials both in terms of rapid readouts and also potentially deriving the most benefit.

The inter- and intragrader reliability of EZ area and transverse EZ measurements in this study were consistently excellent. The annual rate of transverse EZ loss was 10.2 ± 9.9%/y and the annual rate of area of EZ loss was significantly higher at 19.4 ± 16.3%/y. Although both measurements are assessing the EZ, measuring transverse EZ loss is considerably quicker as only a single image is analyzed. In contrast, EZ area measurements require several B-scans to be analyzed and therefore the resulting value is based on more than a single measurement. Assessing the area of EZ loss is more time consuming yet evidently may be twice as sensitive in measuring progression in children compared with measuring transverse EZ loss. Furthermore, the area of EZ loss may provide greater statistical power to detect significant differences in a given sample and may also be a more robust outcome measure in observational studies or therapeutic trials. There are other potential endpoints derived from SD-OCT measurements under investigation in STGD1, including total macular volume.[28]

The annual rate of area of EZ loss showed a stronger correlation with the baseline measurement compared with the annual rate of transverse EZ loss; suggesting the area of EZ may be more valuable in assessing prognosis—with baseline EZ area better predictive of progression than baseline EZ width. However, both baseline measurements showed a weak negative correlation with age at baseline. These findings are in keeping with younger children presenting with larger width and area of EZ loss at baseline, leading to a higher annual rate of EZ loss. In other words, subjects with earlier onset present with a severe and rapidly progressive phenotype at the photoreceptor microstructural level, in keeping with other clinical parameters.[4] Given this greater rate of progression in children, they represent good candidates for therapeutic intervention, thereby highlighting the need to initiate structural assessments in cohorts of young children.

Interocular symmetry in terms of baseline measurements, follow-up measurements, and annual rate

of loss was observed. Although both EZ measurements showed a strong correlation and no significant difference between eyes in the baseline measurement, follow-up measurement, and annual rate of loss, the EZ area measurements consistently showed a higher correlation between eyes. This is valuable for future treatment strategies both for stratification, because both eyes appear to have comparable potential as well as for the use of the nontreated eye as 'control'.

Image quality affected subsequent analysis for both transverse and area EZ measurements. Poor image quality makes EZ borders on line scans less distinct. In addition, because scans for 15% of the subjects were excluded from analysis as the initial loss extended beyond the scan area, it is important to be aware of this potential limitation of the testing device for children with a severe phenotype/high rate of progression and those at advanced stages of disease. Widefield SD-OCT and swept-source OCT imaging may help address this limitation.

In conclusion, this is the first prospective study on the quantification of EZ loss in children with molecularly confirmed STGD1 and highlights the utility of SD-OCT in measuring EZ loss in young subjects. In this cohort, measuring the area of EZ loss was more sensitive compared with transverse EZ loss measurements, and will be valuable both for monitoring disease progression and clinical trials requiring a robust structural outcome measure.

Acknowledgments

Supported by grants from the National Institute for Health Research Biomedical Research Centre at Moorfields Eye Hospital NHS Foundation Trust and UCL Institute of Ophthalmology, Macular Society (UK), Fight for Sight (UK), Onassis Foundation, Leventis Foundation, The Wellcome Trust (099173/Z/12/Z), Moorfields Eye Hospital Special Trustees, Moorfields Eye Charity, Retina UK, and the Foundation Fighting Blindness (USA).

Disclosure: **P. Tanna**, None; **M. Georgiou**, None; **R.W. Strauss**, None; **N. Ali**, None; **N. Kumaran**, None; **A. Kalitzeos**, None; **K. Fujinami**, None; **M. Michaelides**, MeiraGTx (C)

*Preena Tanna and Michalis Georgiou contributed equally and should be considered equivalent authors.

References

1. Tanna P, Strauss RW, Fujinami K, Michaelides M. Stargardt disease: clinical features, molecular genetics, animal models and therapeutic options. *Br J Ophthalmol*. 2017;101:25–30.
2. Michaelides M, Hunt DM, Moore AT. The genetics of inherited macular dystrophies. *J Med Genet*. 2003;40:641–650.
3. Fujinami K, Lois N, Davidson AE, et al. A longitudinal study of stargardt disease: clinical and electrophysiologic assessment, progression, and genotype correlations. *Am J Ophthalmol*. 2013;155:1075–1088.e1013.
4. Fujinami K, Zernant J, Chana RK, et al. Clinical and molecular characteristics of childhood-onset Stargardt disease. *Ophthalmology*. 2015;122:326–334.
5. Strauss RW, Ho A, Munoz B, et al. The natural history of the progression of atrophy secondary to Stargardt Disease (ProgStar) Studies: design and baseline characteristics: ProgStar Report No. 1. *Ophthalmology*. 2016;123:817–828.
6. Burke TR, Tsang SH. Allelic and phenotypic heterogeneity in ABCA4 mutations. *Ophthalmic Genet*. 2011;32:165–174.
7. Lambertus S, van Huet RA, Bax NM, et al. Early-onset stargardt disease: phenotypic and genotypic characteristics. *Ophthalmology*. 2015;122:335–344.
8. Fishman GA, Stone EM, Grover S, Derlacki DJ, Haines HL, Hockey RR. Variation of clinical expression in patients with Stargardt dystrophy and sequence variations in the ABCR gene. *Arch Ophthalmol*. 1999;117:504–510.
9. Fujinami K, Lois N, Mukherjee R, et al. A longitudinal study of Stargardt disease: quantitative assessment of fundus autofluorescence, progression, and genotype correlations. *Invest Ophthalmol Vis Sci*. 2013;54:8181–8190.
10. Allikmets R, Singh N, Sun H, et al. A photoreceptor cell-specific ATP-binding transporter gene (ABCR) is mutated in recessive Stargardt macular dystrophy. *Nat Genet*. 1997;15:236–246.
11. Fujinami K, Zernant J, Chana RK, et al. ABCA4 gene screening by next-generation sequencing in a British cohort. *Invest Ophthalmol Vis Sci*. 2013;54:6662–6674.
12. Haji Abdollahi S, Hirose T. Stargardt-Fundus flavimaculatus: recent advancements and treatment. *Semin Ophthalmol*. 2013;28:372–376.
13. Zernant J, Schubert C, Im KM, et al. Analysis of the ABCA4 gene by next-generation sequencing. *Invest Ophthalmol Vis Sci*. 2011;52:8479–8487.

14. Cideciyan AV, Aleman TS, Swider M, et al. Mutations in ABCA4 result in accumulation of lipofuscin before slowing of the retinoid cycle: a reappraisal of the human disease sequence. *Hum Mol Genet*. 2004;13:525–534.
15. Tsybovsky Y, Molday RS, Palczewski K. The ATP-binding cassette transporter ABCA4: structural and functional properties and role in retinal disease. *Adv Exp Med Biol*. 2010;703:105–125.
16. Charbel Issa P, Barnard AR, Singh MS, et al. Fundus autofluorescence in the Abca4(-/-) mouse model of Stargardt disease–correlation with accumulation of A2E, retinal function, and histology. *Invest Ophthalmol Vis Sci*. 2013;54:5602–5612.
17. Molday RS, Zhang K. Defective lipid transport and biosynthesis in recessive and dominant Stargardt macular degeneration. *Prog Lipid Res*. 2010;49:476–492.
18. Weng J, Mata NL, Azarian SM, Tzekov RT, Birch DG, Travis GH. Insights into the function of Rim protein in photoreceptors and etiology of Stargardt's disease from the phenotype in abcr knockout mice. *Cell*. 1999;98:13–23.
19. Chen Y, Ratnam K, Sundquist SM, et al. Cone photoreceptor abnormalities correlate with vision loss in patients with Stargardt disease. *Invest Ophthalmol Vis Sci*. 2011;52:3281–3292.
20. Gomes NL, Greenstein VC, Carlson JN, et al. A comparison of fundus autofluorescence and retinal structure in patients with Stargardt disease. *Invest Ophthalmol Vis Sci*. 2009;50:3953–3959.
21. Sparrow JR, Boulton M. RPE lipofuscin and its role in retinal pathobiology. *Exp Eye Res*. 2005;80:595–606.
22. Arepalli S, Traboulsi EI, Ehlers JP. Ellipsoid zone mapping and outer retinal assessment in Stargardt disease. *Retina*. 2018;38:1427–1431.
23. Sodi A, Mucciolo DP, Cipollini F, et al. En face OCT in Stargardt disease. *Graefes Arch Clin Exp Ophthalmol*. 2016;254:1669–1679.
24. Park JC, Collison FT, Fishman GA, et al. Objective analysis of hyperreflective outer retinal bands imaged by optical coherence tomography in patients with Stargardt disease. *Invest Ophthalmol Vis Sci*. 2015;56:4662–4667.
25. Cai CX, Light JG, Handa JT. Quantifying the rate of ellipsoid zone loss in Stargardt disease. *Am J Ophthalmol*. 2018;186:1–9.
26. Khan KN, Kasilian M, Mahroo OAR, et al. Early patterns of macular degeneration in ABCA4-associated retinopathy. *Ophthalmology*. 2018;125:735–746.
27. Abed E, Placidi G, Calandriello L, et al. Correlation of macular focal electroretinogram with ellipsoid zone extension in Stargardt disease. *J Ophthalmol*. 2017;2017:3643495.
28. Strauss RW, Munoz B, Wolfson Y, et al. Assessment of estimated retinal atrophy progression in Stargardt macular dystrophy using spectral-domain optical coherence tomography. *Br J Ophthalmol*. 2016;100:956–962.